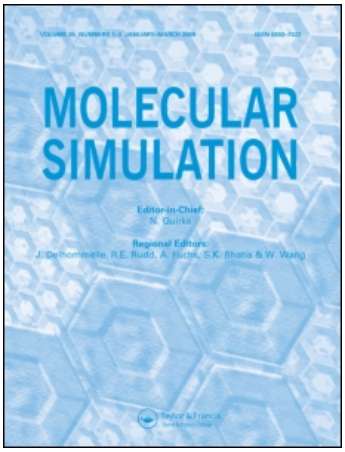

Molecular Simulation
Publication details, including instructions for authors and subscription information:
http://www.informaworld.com/smpp/title~content=t713644482

Incorporation of impurity anions into DSP: insights into structure and stability from computer modelling

J. L. Lowe[a]; A. L. Rohl[ab]; J. D. Gale[a]; P. G. Smith[c]; G. M. Parkinson[a]
[a] AJ Parker Co-operative Research Centre for Hydrometallurgy, Nanochemistry Research Institute, Curtin University of Technology, Bentley, WA, Australia [b] iVEC, Kensington, WA, Australia [c] AJ Parker Co-operative Research Centre for Hydrometallurgy, CSIRO Minerals, Waterford, WA, Australia

To cite this Article Lowe, J. L. , Rohl, A. L. , Gale, J. D. , Smith, P. G. and Parkinson, G. M.(2006) 'Incorporation of impurity anions into DSP: insights into structure and stability from computer modelling', Molecular Simulation, 32: 1, 35 — 44
To link to this Article: DOI: 10.1080/08927020500529301
URL: http://dx.doi.org/10.1080/08927020500529301

Molecular Simulation, Vol. 32, No. 1, 15 January 2006, 35–44

Taylor & Francis
Taylor & Francis Group

Incorporation of impurity anions into DSP: insights into structure and stability from computer modelling

J. L. LOWE†*, A. L. ROHL†,‡, J. D. GALE†, P. G. SMITH§ and G. M. PARKINSON†

†AJ Parker Co-operative Research Centre for Hydrometallurgy, Nanochemistry Research Institute, Curtin University of Technology, Kent Street, Bentley, WA 6102, Australia
‡iVEC, 26 Dick Perry Avenue, Technology Park, Kensington, WA 6151, Australia
§AJ Parker Co-operative Research Centre for Hydrometallurgy, CSIRO Minerals, Conlon Street, Waterford, WA 6152, Australia

(Received October 2005; in final form December 2005)

DSP is an important by-product of alumina production via the Bayer process. Under Western Australian processing conditions, the DSP has a sodalite-type structure that can incorporate anions within its framework. This is particularly useful for removal of impurity anions from liquor recycled in the circuit. As a first step to gaining a fundamental understanding of the incorporation process, we have undertaken molecular mechanics calculations to examine the interaction energy between a series of anions and the sodalite framework, as a measure of the affinity of the anions for the sodalite cage. Our calculations predict that the ions have an increased affinity for the cage along the series aluminate, chloride, carbonate, sulfate and hydroxide. These calculations have successfully predicted the trends that we observe from competitive-uptake experiments in our laboratory.

Keywords: Desilication product; Interaction energy; Binding; Bayer process

1. Introduction

Alumina production via the Bayer process is a major industry in Western Australia (WA) and contributed approximately A$885 million to the value of the WA resource sector in the quarter ended March 2004 [1]. Australia is the worlds leading producer of alumina and during 2004 exports of aluminium and alumina product reached an estimated A$7.4 billion in value [2].

The Bayer process is used exclusively in Australia to refine alumina (Al_2O_3) from bauxite ore through a four-step process:

- digestion of the ore, through heating in hot caustic solution at elevated temperatures and pressures to dissolve the aluminium-bearing minerals;
- clarification of the resultant slurry, to separate out undissolved components of the ore from the aluminium-rich solution;
- crystallisation of aluminium hydroxide through cooling and seeding; and
- calcination of the aluminium hydroxide to produce the final alumina product, with recycling of the remaining caustic liquor.

In addition to the major steps of the process, there may be a slurry storage stage prior to digestion, during which the crushed ore is held at an elevated temperature (lower than that of digestion) for an extended period. The majority of "reactive silica" (predominantly aluminosilicate clays) will dissolve and re-precipitate during this initial storage stage as sodium aluminosilicate desilication product (DSP).

DSP has a sodalite-type structure under processing conditions prevalent in WA and impurity anions can incorporate into its cage structure during precipitation. Incorporation of anions such as carbonate, sulfate and chloride into precipitated DSP is an important mechanism

*Corresponding author. Email: j.lowe@curtin.edu.au

Molecular Simulation
ISSN 0892-7022 print/ISSN 1029-0435 online © 2006 Taylor & Francis
http://www.tandf.co.uk/journals
DOI: 10.1080/08927020500529301

for removal of inorganic impurities from the recycled Bayer liquor.

This research extends our earlier experimental work on the inclusion of selected anions into DSP [3] and builds on the work of Riley *et al.* [4], which produced an empirical model to describe competitive uptake of selected anions that is used in the prediction of plant impurity concentrations. The present study aims to generate a more fundamental understanding of the incorporation process. We are working toward development of a mechanistic model to represent precipitation of DSP, which is a dynamic, non-equilibrium process, similar to many others encountered by industry.

Studies of adsorbed molecules in zeolites have been undertaken using computational techniques for a number of years. Commencing in the 1980s, studies looking at sites of adsorption were undertaken using molecular mechanics, with force-fields based on the work of Kiselev [5]. Later, Monte Carlo techniques proved very useful as they yielded information on the temperature and composition dependence of thermochemical properties. During the late 1980s, molecular dynamics calculations were also undertaken, which allowed time-dependent parameters of the studied system to be examined. In parallel, quantum mechanical techniques have been employed to allow characterisation of active sites and reaction mechanisms [6]. These techniques have been successfully utilised by various researchers, allowing outcomes such as design of structure-directing agents for the synthesis of microporous solids [7].

As a first step along the path of understanding anion interactions within DSP, we have used the interaction energies of selected anions with the zeolite cage as a measure of their affinity for the cage. Calculations on the strength of these types of interactions have been used successfully by Lewis *et al.* [8] as a guide to the efficacy of a selected molecule in templating a specific zeolite framework. We have determined the interaction energies in the first instance by using molecular mechanics calculations. Sensitivity of results to the charges utilised in the system description can be a concern when using this type of calculation on polar systems. Mabilia *et al.* [9] tested the effect of electrostatic potential energy on the relative stabilities of minimum energy structures in their study of the sodalite cage. These authors found that although absolute energies were influenced by the choice of charge, all other energy contributions remained relatively constant and there was no significant impact on the optimised geometries due to charge. We have chosen to use partial charges in our description of the sodalite framework, as they have been shown to provide an accurate description of absorption spectra [10] and to reproduce the order of magnitude of host-guest interaction energies [11] in zeolite structures. The only deficiency of the partial charge, rigid-ion model is the failure to predict low symmetry distortions of silica frameworks in a small number of cases, such as silicalite. However, this does not affect sodalite and this structural effect is secondary to the requirement of describing molecular binding correctly.

This paper outlines the results of our molecular mechanics calculations and compares the optimised structures obtained to those derived from diffraction studies published in the literature. There is additionally some discussion of quantum mechanical calculations that were undertaken to verify our molecular mechanics results.

2. Methodology

Initial crystallographic coordinates for the sulfate, carbonate and hydroxide-containing sodalite-type structures (referred to hereafter simply as sodalite structures) were taken from the literature [12–14]. In the carbonate-containing sodalite, the carbonate is rotationally disordered and a single orientation was chosen, whilst in the sulfatic sodalite, water molecules in the cages not containing sulfate were removed. The hydroxide structure was utilised as reported in the literature. The aluminate and chloride-containing sodalite models were constructed using the framework from the sulfate-containing structure, with insertion of the relevant ion structure within the framework cavity. Once the full unit cells had been generated, the symmetry was converted to the triclinic, P1, description. All coordinates were fully relaxed during the optimisation.

Energies of structures were minimised within the GULP code [15], using the Newton–Raphson/BFGS minimiser with a switch to the rational function optimiser once a gradient norm of less than $0.1\,\mathrm{eV\AA^{-1}}$ was obtained in order to ensure that the Hessian is positive definite for the final structure. The force-field potentials were made up of expressions describing the framework interactions, intramolecular interactions of the cage-filling anions and framework-anion interactions. Framework interactions were described by a series of Buckingham potentials [16]. Intramolecular potentials for each ion were described by a combination of harmonic and Morse potentials, with an improper torsion potential also used to describe the carbonate ion [17–20]. Non-bonding interactions of the framework with the cage-filling anions were described via the Coulomb sum for the partial charges and Lennard–Jones potentials for the Pauli repulsion and van der Waals terms [17]. All potential forms and parameters, as well as atomic charges, are given in the Appendix.

We have used the non-bonding interactions of the respective anions with the sodalite framework (binding energies) as a measure of the affinity of the framework for each anion. The binding energy is given by:

$$E(\text{binding}) = [E(\text{unsolvated ion-containing sodalite})] - [E(\text{empty sodalite framework}) + E(2 \times \text{Na}^+\text{ions}) + E(\text{anion})^* + E(\text{solvation of anion})^* + E(\text{solvation of } 2 \times \text{Na}^+\text{ions})]$$

* values doubled for univalent anions so that calculations effectively compare structures with two univalent anions or a single divalent anion, with addition of two sodium ions to all structures to maintain charge balance

Solvation energies were determined using the COSMO algorithm of Klamt and Schueuermann [21], which is based on a dielectric continuum model of the solvent. The dielectric value selected was that for water (78.4) and the solvent radius was set to 1Å.

The framework potentials and those used for the ionic species have been well-tested on various structures by their developers. It was necessary to convert the potentials for carbonate of Pavese *et al.* [19,21] from a core/shell model to a core only model, in order to ensure consistency with the other components of our force-field where shell model parameterisations were not available. We have used the CVFF force-field to describe the framework-to-anion potentials. However, these were difficult to test since relevant experimental data were not readily available.

In addition, we performed optimisations of each anion-containing structure using density functional theory (DFT) calculations utilising the SIESTA methodology [23–25]. These calculations employed the non-local density functional of Perdew *et al.* [26]. For all elements, core electrons were represented by norm-conserving non-local pseudopotentials. A double-zeta basis set including polarisation functions was used to describe the valence orbitals of chlorine, hydrogen and carbon. The basis set here is numerical and consists of the exact solutions of the pseudopotential for the atomic state, divided in a smooth fashion to create multiple zetas. A radial confinement localises the orbital, corresponding to an orbital energy shift of 0.01 Ry, and a split-norm value of 0.15 was used. Basis sets for the remaining elements were taken from previous work having been optimised according to the procedure described by Anglada *et al.* [27]. Full details of the SIESTA parameters are given in the Appendix. Calculations were performed with a mesh cutoff of 250 Ry for the integration of the Hartree and exchange-correlation energies.

3. Results and discussion

3.1 Stability of anions within the sodalite framework

In our initial binding energy calculations, we predicted the order of stability of the selected anions within the sodalite framework without accounting for the solvation of the guest ions in solution. Our calculations suggest that carbonate is the most-stable anion within the framework and that hydroxide and sulfate anions have a similar stability, followed by chloride and aluminate anions, respectively (table 1).

Table 1. Binding energies of anions within the DSP framework.

	Binding energy ($kJ\,mol^{-1}$)	*Binding energy with solvation* ($kJ\,mol^{-1}$)
Hydroxide	−2206	−502
Sulfate	−2206	−443
Carbonate	−2361	−426
Chloride	−1817	−399
Aluminate	−1603	−255

Upon incorporation of solvation effects into the binding calculations, the order of stability is significantly altered and becomes consistent with the trend from our laboratory results. In the laboratory, we performed competitive uptake experiments, where amounts of each of the sodium salts of carbonate, sulfate and chloride were added to a caustic aluminate solution in such a way that the total ionic strength for each of the anionic species was constant. Kaolin was added and the solution was heated at 95°C. Solid and liquor samples were collected at fixed intervals and subsequently subjected to chemical analyses described elsewhere [3]. These experiments showed that sulfate was by far the dominant inclusion within the sodalite framework, with approximately 2/3 of cage pairs containing a sulfate anion. DSP produced from an additional competitive uptake experiment, with added chloride and carbonate ions only, showed a slight preference for uptake of carbonate ions, with approximately 3/8 of cage pairs containing a carbonate ion and 1/4 of cage pairs containing a pair of chloride ions. Each pair of cages can contain a maximum of one divalent anion, or two univalent anions in order to maintain the charge balance of the overall structure.

The solvated binding energy calculations predicted hydroxide to be the most stable anion within the sodalite framework (table 1). In decreasing order of stability, we calculated that hydroxide is followed by sulfate, carbonate, chloride and finally aluminate ions. Experimentally, however, the stability of hydroxide and aluminate anions within the sodalite cage may not be compared directly to sulfate, carbonate or chloride anions, since aluminate and hydroxide ions may take part in species forming the sodalite framework and hence their availability for inclusion within the forming framework cage is difficult to accurately assess. Additionally, these ions are present in different concentration ranges to the other anions, which makes any comparison difficult.

The percentage of each sodalite-anion species, as a function of the Boltzmann population was calculated

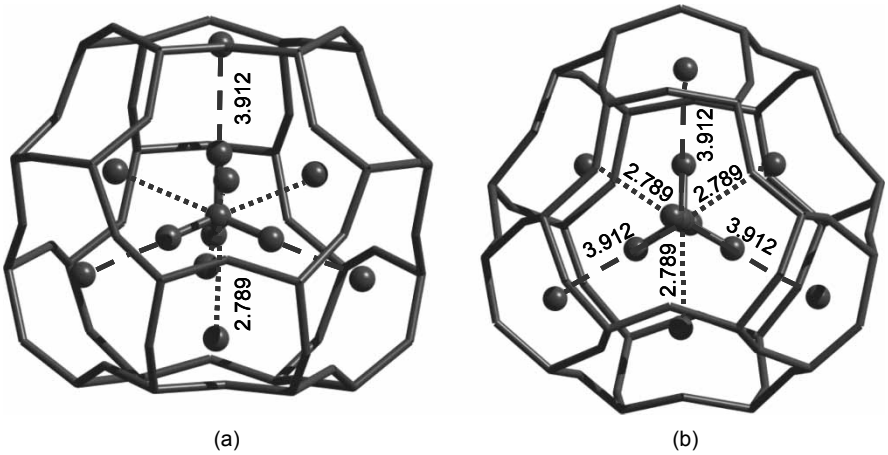

Figure 1. Sulfate anion coordinated by tetrahedra of sodium ions within the nosean structure, viewed from side of cage (a) and from top of cage (b). Dotted lines indicate distance of sodium atoms from sulphur in Angstroms, with line style consistent within each tetrahedron.

using the binding energies from the solvated systems and a temperature of 95°C. Aluminate and hydroxide ions were neglected in this process, for the aforementioned reasons. The calculated percentages were 99.6% sulfate-containing species and 0.4% of the carbonate-containing species, with only negligible levels of the chloride-containing species. The differences in the predicted proportion of anionic species from the modelling, compared to that actually obtained from experiment, may be due in part to the choice of a simple dielectric constant approach to solvation when the solution is likely to contain strong directional bonds involving the anions. Additionally, molecular dynamics studies would be useful for examining the energies of the most highly populated configurations for each anion-sodalite compound at the experimental temperature. Furthermore, the thermodynamics of binding during growth may differ from that within the completed framework, as well as there being the issue of kinetic influences.

3.2 Calculated structures of sodalite-anion materials

3.2.1 Sulfate-containing sodalite structure (nosean). We simulated the sulfate-containing sodalite structure by relaxing the nosean unit cell coordinates described by Hassan and Grundy [12] and optimising the entire system. In our calculated minimum energy structure, the sulfate anion is coordinated by a tetrahedron of sodium ions within the sodalite cage, with a further tetrahedron of sodium ions located within the adjacent empty cages (figure 1). This configuration remains consistent with the ideal structure for nosean reported by Hassan and Grundy [12], which they produced from refinement of X-ray diffraction data for water-containing nosean, followed by further optimisation and minimisation of electrostatic neutrality of their proposed structure.

In our calculated structure, the sodium ions sit closer to the six-membered rings of the framework and the O–Si–O and O–Al–O angles are closer to ideal tetrahedral angles

Table 2. Comparison of modelled nosean structure with ideal structure of Hassan and Grundy [12].

	Hassan et al.	*GULP*	*SIESTA*
Distances			
$S-O_{SO_4}$	*1.504*	1.437	1.536
Na_1-S	*2.591*	2.789	2.826
Na_1-O	2.498* × 3/2.848* × 3	2.382 × 3/3.057 × 3	2.537/3.081
Na_2-S	*4.074*	3.912	4.061
Na_2-O	2.996* × 3/2.256* × 3	3.048 × 3/2.189 × 3	3.045/2.289
O–Si	*1.592*	1.599/1.605†	1.647
O–Al	*1.718*	1.737/1.742†	1.764
Angles			
Si–O–Al	*143.39*	141.39/140.82†	143.6/144.3
O–Si–O	*100.46/112.25*	107.79/108.95	107.29/107.95
O–Al–O	*101.98/112.76*	108.95/109.84	108.15/108.82
4 memb O–Si–O	*109.88*	111.20	113.44
4 memb O–Al–O	*108.13*	109.57	111.40
$O_{SO_4}-S-O_{SO_4}$	*109.47*	109.47	109.47

All distances are in Angstroms and angles in degrees.
Italicised values are our measurements of values not quoted by Hassan and Grundy. We have followed this protocol throughout this paper.† Associated with the four-membered ring.

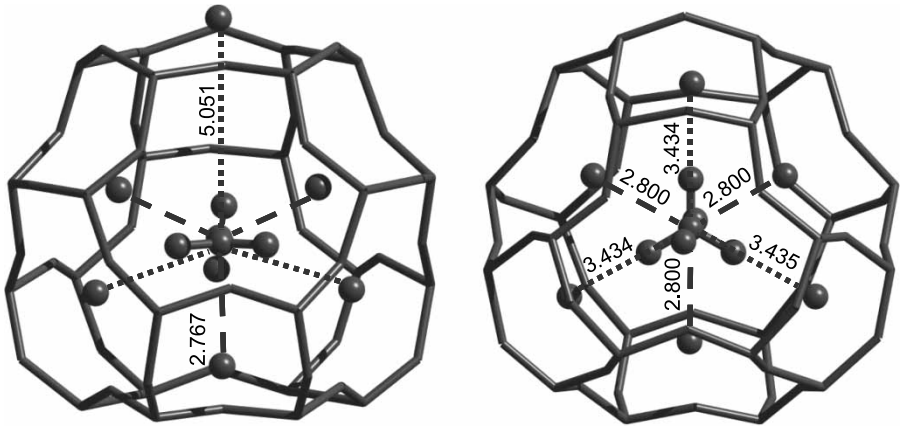

Figure 2. Structure of carbonate anion within the sodalite cage. Dotted lines show position of sodium atoms relative to carbon, with line style consistent for each tetrahedron and distances in Angstroms. Views from side of cage (a) and top of cage (b) show tetrahedral arrangement of sodium about carbonate.

compared with the Hassan and Grundy structure, as shown in table 2. Asterisked measurements in this table are our calculated values, quoted only where we obtained a result that differed by more than the error quoted by Hassan and Grundy. We have followed this protocol in comparing all of the remaining models in this paper. The length of Si–O and Al–O bonds in our model are close to the values quoted by Hassan and Grundy (within 1.1%). Our model predicts S–O bonds in sulfate as slightly shorter (4.5%) than our initial structure although angles are tetrahedral. Our potential set may benefit from further balancing of inter and intra-atomic potentials in order to obtain more accurate bond distances within the anion. We have validated our model using DFT calculations, which produced a structure that gave similar tetrahedral angles to those obtained from the force-field calculations, although it was slightly closer to experimentally-derived angles between Si and Al atoms in adjacent tetrahedra. This model predicted bond lengths that were in general a little larger than those predicted using atomistic methods or derived experimentally by Hassan and Grundy [12], which is characteristic of a GGA functional.

3.2.2 Carbonate-containing sodalite structure. Our simulation found that the sodium ions were arranged about the carbonate anion in such a way as to form two interlinking tetrahedra, similar to nosean, although the tetrahedra in the carbonate-containing structure were subject to distortion (figure 2). Gesing and Buhl [13] reported that four of the eight sodium ions in the structure were contained within the anion-bearing cage, whilst the remaining four were located within the empty cage. In contrast, Sieger *et al.* [28] found that five of the anions were located within the anion-bearing cage, with the remaining three in the empty cage. Our calculations produced a model that contained seven of the eight sodium ions within the carbonate-containing cage. The structure obtained from our atomistic calculations was again validated by DFT calculations, which gave a consistent structure.

Comparing our modelled structure further to the experimentally derived structures of Gesing and Buhl [13] and Sieger *et al.* [28] (table 3), we find that three of the four sodium ions associated with the inner tetrahedron reported by these authors moved outward a short distance (we have denoted these sodium ions as Na_4 in table 3). The remaining sodium ion of this tetrahedron was found at the same relative position as in the experimentally determined structures. The outward shift of three of the sodium ions was along the axis of the C–O bond of the oxygen atom opposite each sodium ion (figure 2(b)).

In addition, we found that three of the four sodium ions associated with the outer tetrahedron reported previously moved so that they were within the carbonate-containing cage (ions denoted as Na_3 in table 3). The position of these ions may be comparable to the additional sodium position reported by Sieger *et al.* [28], although these authors report a lower occupancy at this position.

As a result of our simulation being based on a single conformation of the carbonate molecule within the cage, it has highlighted the impact of the carbonate conformation on the surrounding sodium ions, which may not be demonstrated so clearly with an averaged structure based on multiple carbonate conformations. Differences in the sodium positions of the experimentally-derived structures proposed by Gesing and Buhl [13] and Sieger *et al.* [28] could possibly be due to the differences in the averaged carbonate conformation of their respective samples. Molecular dynamic simulations of the carbonate anion within the sodalite-type cage would shed further light on this issue.

The angles and bond lengths for the sodalite framework in our model are consistent with those reported by Gesing

Table 3. Comparison of modelled carbonate-containing sodalite structure with experimentally-derived structures of Gesing and Buhl [13] and Sieger *et al.* [28].

	Gesing and Buhl	*Sieger et al.*	*GULP*	*SIESTA*
Distances				
Al–O	175 (7) × 2/174 (6) × 2	1.646*/1.779*	1.74/1.74	1.762/1.762
Si–O	160 (6) × 2/161 (6) × 2	1.673*/1.574*	1.60/1.60	1.645/1.647
$C–O_{CO_3}$	1.26 (5) × 2	1.231(9)	1.138	1.312
$C–O_{CO_3}$†	1.29 (5) × 1	–	–	–
C–Na$_1$	2.88 (5) × 4	*2.911 × 4*	2.767 × 1	2.971 × 1
Na_1–O (inner T)	2.44 (4) × *3/3.02*	2.484 × 3*/2.979 × 3*	2.314 × 3/2.996 × 3	2.399/2.994
$Na_1–O_{CO_3}$	2.54 (4) × 2	2.526 × 3*	2.988 × 3	3.257
$Na_1–O_{CO_3}$†	2.40 (4) × 1	–	–	–
C–Na$_2$	*4.225 × 4*	*4.267 × 3*	5.051 × 1	5.130 × 1
Na_2–O (outer T)	2.98 (4) × 3/2.25 (4) × 3	2.976(4) × 3/2.320 × 3*	3.068/2.255	3.041/2.373
$Na_2–O_{CO_3}$	*2.929 × 3*	*3.130 × 3*	5.182	5.284
$Na_2–O_{CO_3}$†	*3.666 × 2*	–	–	–
C–Na$_3$		*3.262 × 1*	3.434 × 3	3.626 × 3
Na_3–O (outer T moved in)	–	3.167*/*2.384 × 3*	3.142/2.219	3.114/2.304
$Na_3–O_{CO_3}$	–	*2.137*	2.356	2.403
C–Na$_4$			2.800 × 3	2.882 × 3
Na_4–O (inner T moved out)	–	–	2.354/3.084	2.501/3.089
$Na_4–O_{CO_3}$	–	–	2.492	2.555
Angles				
Al–O–Si	*144.2/142.9*	147.2*/147.3(3)	139.5/139.5	142.7/142.8
O–Si–O	108(3)/107(3) × 2 108(3) × 2/117(4)	107.6*/107.8(1) × 2 109.2(2) × 2/114.6*	111.1/108.3/112.6	113.7/107.4/113.7
O–Al–O	114(4)/108(3) × 2/109(3) × 2/107(3)	112*/110.8(1) × 2/107.6(2) × 2/107*	109.3/109.3/110.2	111.6/108.3/112.2
$O_{CO_3}–C–O_{CO_3}$	113(4)	120.0	120	120
$O_{CO_3}–C–O_{CO_3}$†	113(4) × 2	–	–	–

All distances are in Angstroms and angles in degrees.† Additional oxygen position determined for carbonate by Gesing and Buhl [13].

and Buhl [13]. We predict that the carbonate anion retains its flat structure, with bond angles of 120° which is consistent with the structure proposed by Sieger *et al.* [28] and in contrast with that reported by Gesing and Buhl [13]. Our bond length for the C–O bond in the carbonate anion is shorter than that reported by both Gesing and Buhl [13] and Sieger *et al.* [28].

3.2.3 Chloride-containing sodalite structure. In our simulated model of the chloride-containing sodalite structure, the chloride ions are coordinated by two tetrahedra of sodium ions, as for the previous structures. In this case, however, the structure is symmetrical, with each cage occupied by a chloride ion. Our model was similar to the experimentally-derived structure reported by Hassan and Grundy [29] except that again we predict that the sodium ions sit closer to the sodalite framework (table 4). The structure is shown in figure 3.

3.2.4 Hydroxide-containing sodalite structure. The hydroxide ions in each cage were coordinated by two tetrahedra of sodium ions, as for the earlier structures. Our modelled structure is similar to the structure proposed by Luger and Felsche [14] (table 5) from refinement of powder neutron diffraction data. As with earlier structures, however, we find that the sodium ions lie closer to the framework than predicted in the literature models. The tetrahedra of sodium ions closest about the hydroxide ion in our model are distorted, due to our use of a single configuration of the hydroxide ion within the sodalite cage. The primary distortion of the tetrahedra is in the line of the hydroxide O–H bond, with the sodium atom (A) along this line moving further from the hydroxide oxygen (figure 4).

3.2.5 Aluminate-containing sodalite structure. In our modelled structure of aluminate-containing sodalite

Table 4. Comparison of modelled chloride-containing sodalite structure with the experimentally-derived structure of Hassan and Grundy [29].

	Hassan and Grundy	*GULP*	*SIESTA*
Distances			
Na_1–Cl	2.736	2.839	2.960
Na_1–O	2.353(2)/3.087(2)	2.283/3.072	2.359/3.078
Na_2–Cl	2.736	2.839	2.960
Na_2–O	3.087(2)/2.353(2)	3.072/2.283	3.078/2.359
O–Si	1.620(2)	1.603	1.646
O–Al	1.742(2)	1.740	1.763
Angles			
Si–O–Al	138.2(1)	137.98	139.62
O–Si–O	113.0(1)/107.7(1)	111.85/108.29	113.78/107.36
O–Al–O	111.0/108.7	109.69/109.36	111.89/108.27

All distances are in Angstroms and angles in degrees.

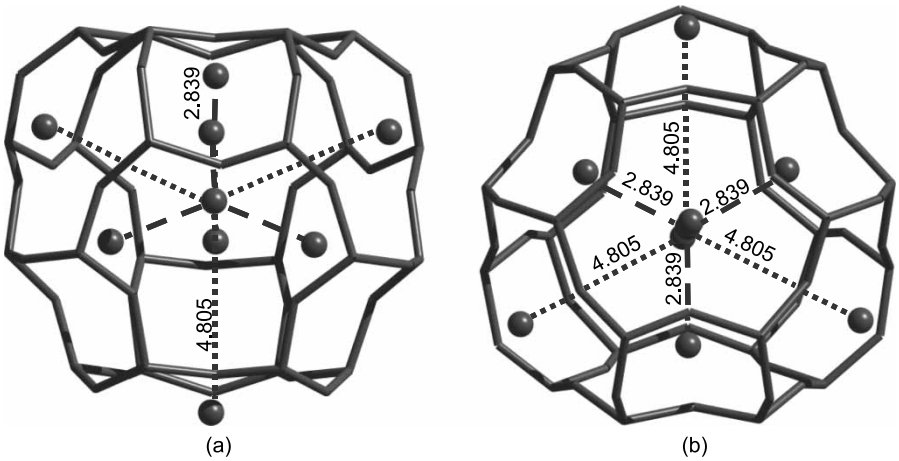

Figure 3. Chloride anion coordinated by tetrahedra of sodium ions within the sodalite cage, as viewed from side of cage (a) and top of cage (b). Distances in Angstroms from chloride to sodium ions are indicated by dotted lines that are consistent for each tetrahedron.

Table 5. Comparison of modelled hydroxide-containing sodalite structure with experimentally-derived structure of Luger and Felsche [14].

	Luger and Felsche	*GULP*	*SIESTA*
Distances			
$O_{OH}-H_{OH}$	1.09	0.980	0.980
$Na-H_{OH}$	2.28	2.374	2.395
$Na-O_{OH}$	2.401	2.393	2.446
Na–O	2.349	2.292	2.399
O–Si	1.635	1.602	1.649
O–Al	1.734	1.737	1.767
Angles			
Si–O–Al	132.9	131.74	133.14
O–Si–O	108.1/112.4	108.78/110.85	107.70/113.09
O–Al–O	108.9/110.6	109.91/108.59	108.67/111.04

All distances in Angstroms and angles in degrees.

(figure 5), the aluminate ion is coordinated by two distorted tetrahedra of sodium ions. There was a significant difference in the conformation of the aluminate anion within the sodalite cage as determined by force-field and DFT calculations (table 6). This is most likely due to the limitations inherent in use of a molecular mechanics force-field in situations that deviate significantly from equilibrium. Neither of the calculated conformations for the aluminate anion gave Al–O–H bond angles similar to those suggested by Adams and Haselden [30] from their Rietveld refinement of the structure of a zeolite A-type structure that contained aluminate ions in the β-cage. From our calculations it is difficult to predict whether the aluminate ion will incorporate readily into the DSP structure. However, our force-field calculations suggest that this is not favourable. Riley *et al.* [4] have suggested inclusion of aluminate ions into the DSP cage, as an explanation for experimentally measured levels of aluminium in DSP that were above that required for the framework alone, working on the assumption that Si:Al ratio in the framework could not be greater than 1 according to Lowenstein's rule.

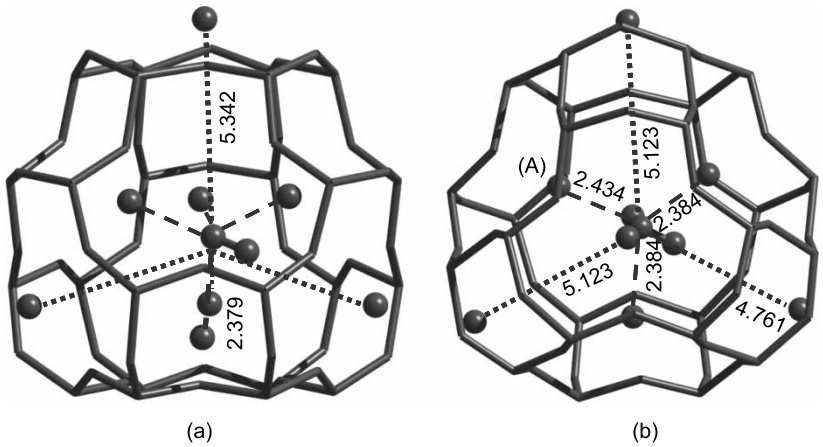

Figure 4. Hydroxide anion within the sodalite cage, coordinated by two tetrahedra of sodium ions as indicated by dotted lines from hydroxide oxygen to sodium atoms. Side of cage view (a) and top of cage view (b) shown, with dotted line style consistent for each tetrahedron and distances in Angstroms.

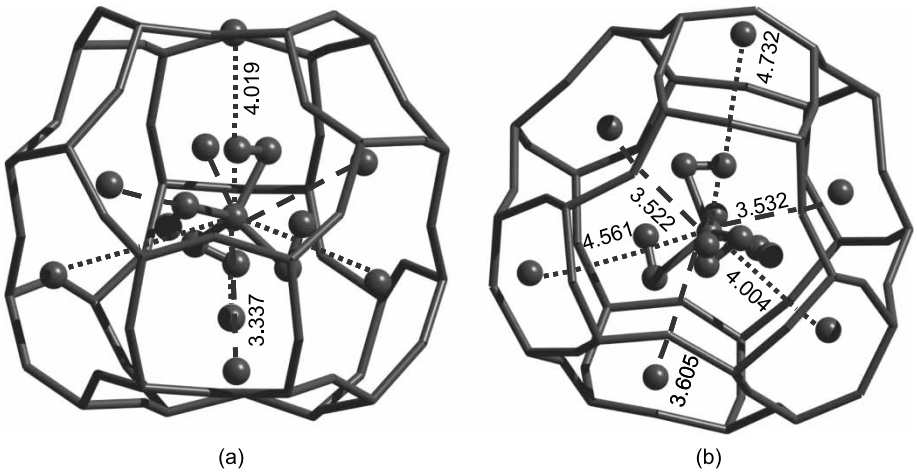

Figure 5. Aluminate anion coordinated by distorted tetrahedra of sodium ions, as indicated by dotted lines of consistent style for each tetrahedron. View shown from side of cage (a) and above cage (b). Distances are given in Angstroms.

Table 6. Modelled aluminate-containing sodalite structure compared with reported structure of β-cage containing aluminate from Adams and Haselden [30].

	Adams and Haselden	*GULP*	*SIESTA*
Distances			
$Al_{alum}-O_{alum}$	1.80	1.644	1.772
$O_{alum}-H_{alum}$	1.00	0.998	0.977
$Na-H_{alum}$	*2.513*	2.916	2.921
$Na-O_{alum}$	*3.104*	2.755	2.732
Na–O	2.327/3.038	2.593	2.699
O–Si	1.582(16)/1.677(11)	1.604	1.647
O–Al	1.653(19)/1.735(12)	1.742	1.766
Angles			
$O_{alum}-Al_{alum}-O_{alum}$	109.5	109.4	109.4
$Al_{alum}-O_{alum}-H_{alum}$	134.1	66.8	111.1
Si–O–Al	132.9(7)/150.5(10)	144.5	149.3
O–Si–O	102.9(7)/104.8(6)	109.3	109.5
O–Al–O	105.6(9)/105.8(7)	109.4	109.4

Distances are given in Angstroms and angles in degrees.

4. Conclusions

We have used molecular mechanics calculations to examine binding energies as a guide to the affinity of anions for a sodalite-type framework. The calculated structures were validated by DFT calculations. We were unable to compare the energetics of the DFT calculations with the molecular mechanics since the isolated anions were unstable in a vacuum and hence the analogous DFT binding energies could not be calculated. Our calculations successfully predicted the trend that we observed from competitive-uptake experiments in the laboratory. Further refinement of the solvent characteristics in our model may allow us to predict more accurately the relative populations of different anion-containing sodalite-type structures than we have currently achieved. Molecular dynamics calculations will also give a greater appreciation of the structures present at the experimental temperature. The final structures have been compared to published, experimentally-derived structures. The carbonate, hydroxide and aluminate-containing structures differed from the published structures, although this was anticipated since our model examined only single anion conformations. Molecular dynamics studies would additionally be of use in examining the behaviour of carbonate and associated sodium ions within the sodalite cage, and our potential set may benefit further from slight adjustments in order to more accurately predict bond distances within the anions.

Acknowledgements

iVEC, the hub of advanced computing in Western Australia provided access to the Australian Partnership for Advanced Computing (APAC) computing resources utilised in this research. J. L. Lowe gratefully acknowledges financial support provided by an Australian postgraduate award (APA) as well as additional funding from the Australian Institute of Nuclear Science and Engineering, iVEC and the AJ Parker CRC for Hydrometallurgy. J. D. Gale gratefully acknowledges funding from the Government of Western Australia through the Premier's Research Fellowship program.

Appendix

Table A1. Atomic charges and force-field potential parameters used in this work.

Atomic charges (a.u.)

Si	2.40000	S	1.360000
Al	1.40000	O_{SO_4}	−0.840000
O_{frame}	−1.20000	H_{OH}	0.400000
Na	1.00000	O_{OH}	−1.400000
Cl	−1.00000	Al	1.147000
C	1.13500	$H_{Al(OH)_4}$	0.423000
O_{CO_3}	−1.04500	$O_{Al(OH)_4}$	−0.959750

Buckingham Aexp^(−*r*/*p*) − *C*/*r*^6 [16]

i	*j*	A_{ij} (eV)	ρ_{ij} (Å^{-1})	C_{ij} (eVÅ^6)	Cutoff (Å)
O_{frame}	O_{frame}	1388.7730	0.362319	175.0000	10
Si	O_{frame}	18003.7572	0.205205	133.5381	10
Al	O_{frame}	16008.5345	0.208478	130.5659	10
Na	O_{frame}	3542.2072	0.241864	0	10

Harmonic $1/2k_2(r - r_\theta)^2$ [17]

I	*j*	k_2 (eVÅ^{-2})	r_θ (Å)
O_{OH}	H_{OH}	46.88699	0.96

Morse $D\{[1 - \exp(-a(r - r_0))]^2 - 1\}$ [18][19][20]

i	*j*	D_{ij} (eV)	a_{ij} (Å^{-1})	r_{0ij} (Å)
C	O_{CO_3}	4.710000	3.800000	1.180000
Al	$O_{Al(OH)_4}$	3.003840	1.463680	1.852950
$O_{Al(OH)_4}$	$H_{Al(OH)_4}$	4.645155	2.183340	0.975200
O_{SO_4}	S	5.000000	1.200000	1.505000

Three body harmonic – cosine $1/2k(\cos\theta - \cos\theta_0)^2$ [18]

H	*I*	*J*	*k* (eV rad^{-2})	θ_0 (deg)
Al	$O_{Al(OH)_4}$	$O_{Al(OH)_4}$	27.124113	117.22000
$O_{Al(OH)_4}$	Al	$H_{Al(OH)_4}$	2.014774	105.81000

Three body harmonic $1/2k(\theta - \theta_0)^2$ [19][20]

H	*I*	*J*	*k* (eV rad^{-2})	θ (deg)
C	O_{CO_3}	O_{CO_3}	1.690000	120.00000
S	O_{SO_4}	O_{SO_4}	15.00000	109.47000

Torsion $k*(1 - \cos(-2*\varphi - \varphi_0))$ [22]

K (eV)	C	O_{CO_3}
0.112900		

Lennard $A_{ij}/r^{12} - B_{ij}/r^6$ [17]

i	O_{frame}	Si	Al	Na	atom	
j	A_{ij}					
O_{CO_3}	325653.2156	927034.7530	8716.1604	135644.9731	O_{CO_3}	272894.7846
C	1074100.2365	3057633.7026	28748.4646	447397.0798	-	-
O_{SO_4}	325653.2156	927034.7530	8716.1604	135644.9731	O_{SO_4}	272894.7846
S	2243.6564	6387.0011	60.0518	934.5546	-	-
Cl	3151161.3737	8970389.2534	84341.3381	1312559.4323	Cl	25552052.0000
O_{OH}	494545.9294	1407820.4714	13236.6009	205994.1867	O_{OH}	629358.0000
Al	10401.2455	29609.1536	278.3910	4332.4512	Al	278.3910
					$O_{Al(OH)_4}$	8716.1604
$O_{Al(OH)_4}$	325653.2156	927034.7530	8716.1604	135644.9731	$O_{Al(OH)_4}$	272894.7846
	B_{ij}					
O_{CO_3}	9.717395704	595.1503575	918.2482231	0.479045142	O_{CO_3}	498.8788
C	15.8407711	970.1818134	1496.878419	0.780913392	-	
O_{SO_4}	9.717395704	595.1503575	918.2482231	0.479045142	O_{SO_4}	498.8788
S	24.90661645	1525.427402	2353.558196	1.227838608	-	
Cl	25.01898902	1532.309758	2364.176876	1.233378316	Cl	3307.0045
O_{OH}	10.88093011	666.4120347	1028.196756	0.536404698	O_{OH}	625.5
Al	17.8860704	1095.447949	1690.14959	0.881741919	Al	1690.14959
					$O_{Al(OH)_4}$	918.2482231
$O_{Al(OH)_4}$	9.717395704	595.1503575	918.2482231	0.479045142	$O_{Al(OH)_4}$	498.8788

Table A2. SIESTA optimised basis set parameters.

Element	*Orbital*	*Zetas*	*Polarisation*	*Comments*
Al	3s	double	none	Soft confinement potential optimised basis of J. Junquera *et al.*, *Phys. Rev. B* 64, 235111 (2001).
	3p	double		
	3d	single		
Si	3s	double	none	Soft confinement potential optimised basis of J. Junquera *et al.*, *Phys. Rev. B* 64, 235111 (2001).
	3p	double		
	3d	single		
O	2s	double	none	Soft confinement potential optimised basis of J. Junquera *et al.*, *Phys. Rev. B* 64, 235111 (2001).
	2p	double		
	3d	single		
Na	2p	double	yes	
	3s	double	no	
	3p	double	no	
S	3s	double	no	
	3p	double	yes	

References

[1] Australian Bureau of Agricultural and Resource Economics (ABARE), *Australian Mineral Statistics, March quarter 2004*, pp. 1–5, ABARE, Australia (2004).

[2] Australian Aluminium Council, *Sustainability Report 2004*, p. 3, AAC, Australia (2004).

[3] P. Smith, J.L. Lowe, A.L. Rohl, G.M. Parkinson. Understanding growth of DSP in the presence of inorganic ions. *Proceedings of the 6th International Alumina Quality Workshop*, 8–13 September 2002, Brisbane Convention & Exhibition Centre, Queensland, Australia (2002).

[4] G. Riley, P. Smith, D. Binet, R. Pennifold. Plant impurity balances and impurity inclusion in DSP. *Proceedings of the Fifth International Alumina Quality Workshop*, Bunbury, Western Australia 2, pp. 404–414 (1999).

[5] A.G. Bezus, A.K. Kiselev, A.A. Lopatkin, P.Q. Du. Molecular statistical calculation of the thermodynamic adsorption characteristics of zeolites using the atom–atom approximation. Part 1.—Adsorption of methane by zeolite NaX. *J. Chem. Soc., Faraday Trans.*, **2**(74), 367 (1978).

[6] C.R.A. Catlow (Ed.). *Modelling of Structure and Reactivity in Zeolites*, pp. 63–78, Academic Press, London (1992).

[7] D.W. Lewis, D.J. Willock, C.R.A. Catlow, J.M. Thomas, G.J. Hutchings. *De novo* design of structure-directing agents for the synthesis of microporous solids. *Nature*, **382**, 604 (1996).

[8] D.W. Lewis, C.R.A. Catlow, J.M. Thomas. Application of computer modelling to the mechanisms of synthesis of microporous catalytic materials. *Faraday Discuss.*, **106**, 451 (1997).

[9] M. Mabilia, R.A. Pearlstein, A.J. Hopfinger. Molecular modeling of zeolite structure. 1. Properties of the sodalite cage. *J. Am. Chem. Soc.*, **109**, 7960 (1987).

[10] N.P. Blake, V.I. Srdanov, G.D. Stucky, H. Metiu. A model for electron–zeolite Na+–zeolite interactions: frame charges and ionic sizes. *J. Phys. Chem.*, **99**, 2127 (1995).

[11] G. Ricchiardi, J.M. Newsam. Predicted effects of site-specific aluminum substitution on the framework geometry and unit cell dimensions of zeolite ZSM-5 materials. *J. Phys. Chem. B*, **101**, 9943 (1997).

[12] I. Hassan, H.D. Grundy. The structure of nosean, ideally $Na_8[Al_6Si_6O_{24}]SO_4.H_2O$. *Can. Mineral.*, **27**, 165 (1989).

[13] T.M. Gesing, J.C. Buhl. Crystal structure of a carbonate-nosean $Na_8[AlSiO_4]_6CO_3$. *Eur. J. Mineral.*, **10**, 71 (1998).

[14] S. Luger, J. Felsche, P. Fischer. Structure of hydroxysodalite $Na_8[AlSiO_4]_6(OH)_2$, a powder neutron diffraction study at 8 K. *Acta Crystallogr.*, **C43**, 1 (1987).

[15] J.D. Gale. GULP: a computer program for the symmetry-adapted simulation of solids. *J. Chem. Soc., Farad. Trans.*, **93**(4), 629 (1997).

[16] G.J. Kramer, N.P. Farragher, B.W.H. van Beest, R.A. van Santen. Interatomic force fields for silicas, aluminophosphates and zeolites: derivation based on *ab initio* calculations. *Phys. Rev. B*, **43**(6), 5068 (1991).

[17] Accelrys, CVFF force-field located within Insight II program, available at http://www.accelrys.com. (2002).

[18] Accelrys, ESFF force-field located within Insight II program, available at http://www.accelrys.com. (2002).

[19] A. Pavese, M. Catti, S.C. Parker, A. Wall. Modelling of the thermal dependence of structural and elastic properties of calcite, $CaCO_3$. *Phys. Chem. Miner.*, **23**, 89 (1996).

[20] N.L. Allan, A.L. Rohl, D.H. Gay, C.R.A. Catlow, R.J. Davey, W.C. Mackrodt. Calculated bulk and surface properties of sulfates. *Farad. Discuss., Cryst. Growth*, **95**, 273 (1993).

[21] A. Klamt, G. Schueuermann. COSMO: a new approach to dielectric screening in solvents with explicit expressions for the screening energy and its gradient. *J. Chem. Soc., Perkin Trans.*, **2**, 799 (1993).

[22] A. Pavese, M. Catti, G.D. Price, R.A. Jackson. Interatomic potentials for $CaCO_3$ polymorphs (calcite and aragonite), fitted to elastic and vibrational data. *Phys. Chem. Miner.*, **19**, 80 (1992).

[23] J.M. Soler, E. Artacho, J.D. Gale, A. Garcia, J. Junquera, P. Ordejon, D. Sanchez-Portal. The SIESTA method for *ab initio* order-*N* materials simulation. *J. Phys.: Condens. Matter*, **14**, 2745 (2002).

[24] E. Artacho, D. Sanchez-Portal, P. Ordejon, A. Garcia, J.M. Soler. Linear-scaling *ab-initio* calculations for large and complex systems. *Phys. Status Solid. (B)*, **215**, 809 (1999).

[25] D. Sanchez-Portal, P. Ordejon, E. Artacho, J.M. Soler. Density-functional method for very large systems with LCAO basis sets. *Int. J. Quantum Chem.*, **65**, 453 (1997).

[26] J.P. Perdew, K. Burke, M. Ernzerhof. Generalized gradient approximation made simple. *Phys. Rev. Lett.*, **77**, 3865 (1996).

[27] E. Anglada, J.M. Soler, J. Junquera, E. Artacho. Systematic generation of finite-range atomic basis sets for linear-scaling calculations. *Phys. Rev. B*, **66**(20), 205101 (2002).

[28] P. Sieger, A.M. Schneider, M. Wiebcke, P. Behrens, J. Felsche. Synthesis and structural characterization of sodalites with acetate and formate guest anions, $[Na_4(CH_3COO)]_2[Al_3Si_3O_{12}]_2$ and $[Na_4(HCOO)_2[Al_3Si_3O_{12}]_2$ and their intracage oxidation product $[Na_5(CO_3)][Na_3.box][Al_3Si_3O_{12}]_2^1$. *Chem. Mater.*, **7**, 163 (1995).

[29] I. Hassan, H.D. Grundy. The crystal structures of sodalite-group minerals. *Acta. Crystallogr.*, **B40**, 6 (1984).

[30] J.M. Adams, D.A. Haselden. The structure of a carbon monoxide adduct of cobalt-exchanged zeolite A ($Co_{5.25}Na_{1.5}$–A.1.5CO) by neutron profile refinement. *J. Solid State Chem.*, **55**, 209 (1984).